ACS APPLIED MATERIALS & INTERFACES

Research Article

Cite This: ACS Appl. Mater. Interfaces 2019, 11, 15656−15661

www.acsami.org

Full-Cell Cycling of a Self-Supporting Aluminum Foil Anode with a Phosphate Conversion Coating

Mengwen Jiang,[†,‡] Yue Yu,[†,‡] Huimin Fan,[†,‡] Hui Xu,[†,‡] Yuheng Zheng,[†,‡] Yunhui Huang,[†,‡] Sa Li,[*,†,‡] and Ju Li[*,§]

[†]School of Materials Science and Engineering and [‡]Institute of New Energy for Vehicles, Tongji University, Shanghai 201804, China

[§]Department of Nuclear Science and Engineering and Department of Materials Science and Engineering, Massachusetts Institute of Technology, Cambridge, Massachusetts 02139, United States

Supporting Information

ABSTRACT: Aluminum foil is a promising candidate anode material for lithium-ion batteries (LIBs), due to its high theoretical capacity, low lithiation voltage, and abundance. However, as a matter of fact, it has been a great challenge to make Al foil cycle in full cells at industrially acceptable areal capacities of 2−4 mAh/cm^2 for commercial 18650 LIBs and some high-power LIBs. In this study, we defined the concepts of electrochemical true contact area (ECA) (areas with perfect electrolyte/electrode contact) and electrochemical noncontact area (ENA) (referred to regions without electrolyte spread on) for the metal foil anode. An initial ECA/ENA partition would cause severe inhomogeneity of the alloying reaction, cause localized electrode pulverization, and exacerbate ECA/ENA inequality even more. Through a phosphate conversion coating on aluminum foil, we killed two birds with one stone: first, the Al foil with a phosphate conversion coating has improved wettability (characterized by the contact angle that decreased from 35.2 to 15.9°) and favors the elimination of ENA, thus guaranteeing uniform electrochemical contact; also, the coating functions as an artificial solid electrolyte interface, which stabilizes the fragile naturally formed solid electrolyte interface and a "steady-state" electrolyte/electrode interface. Therefore, when pairing the phosphated Al foil anode against a commercial $LiFePO_4$ (LFP) cathode (with ~2.65 mAh/cm^2), it can cycle 120 times without Li excess and stabilizes at 1.27 mAh/cm^2.

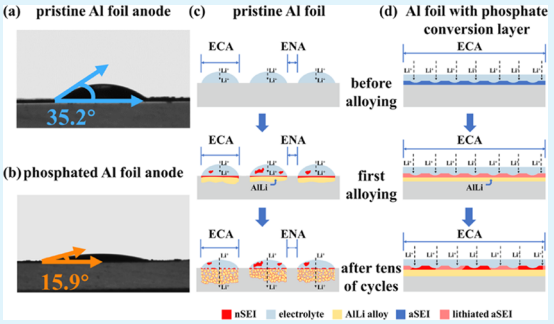

KEYWORDS: *aluminum foil anode, phosphate conversion coating, lithium-ion batteries, full cell, artificial SEI (aSEI)*

1. INTRODUCTION

Aluminum should be one of the best anode materials for LIBs, due to its high theoretical capacity (993 mAh/g if lithiated to AlLi),[1] low electrochemical potential (~0.2−0.45 V vs Li^+/Li), low cost (~\$2 kg^{-1}),[2] superior electrical conductivity, and so on. While most efforts were devoted to nanostructured Al electrodes,[2,3] the inherent drawback of high surface area that usually leads to a large amount of electrolyte decomposition and inadequacy in tap density that causes poor volumetric energy has overshadowed the above-mentioned advantages of Al anodes. Therefore, Al foil, which is fully dense and self-supporting and can be produced in large quantities by roll-to-roll processing, should be an attractive anode for rechargeable lithium-ion batteries. Although some attempts were made to apply Al foil anodes into LIBs,[4] the result of full-cell cycling is quite disappointing. In particular, when paired against cathodes with industrially acceptable areal capacities of 2−4 mAh/cm^2 for commercial 18650 LIBs and some high-power LIBs, deeply charged/discharged, serious degradation is observed. It is commonly believed that the failure of Al foils in full cells could be ascribed to pulverization due to repeated volume expansion/shrinkage during charging/discharging.

Curiously, we disassembled an Al//Li half-cell that was cycled 7 times without further electrolyte washing and found several large unreacted regions (marked as the blue region in Figure 1a,b), where no energy-dispersive X-ray spectroscopy (EDS) signals of electrolyte's solvent or salt were detected (Figure S1a), and some "corroded" areas (marked as the red region in Figure 1a,b) with cracked mudlike bumps composed of fluorine-containing compounds (Figure S1b) were randomly distributed. We speculate that this is due to liquid electrolyte wetting issue, and to help the discussion, we conceptually divide the Al foil into an electrochemical true contact area (ECA) (referred to regions with perfect liquid electrolyte/electrode contact) and an electrochemical noncontact area (ENA) (referred to regions without liquid electrolyte). The term "true contact area" is to distinguish from the "nominal contact area".[5] Generally speaking, particulate-based anodes, especially nanoparticles, have much larger ECA (unit m^2/kg) than foil anodes, which can decrease solid-state lithium

Received: February 15, 2019
Accepted: April 5, 2019
Published: April 5, 2019

DOI: 10.1021/acsami.9b02813
ACS Appl. Mater. Interfaces 2019, 11, 15656−15661

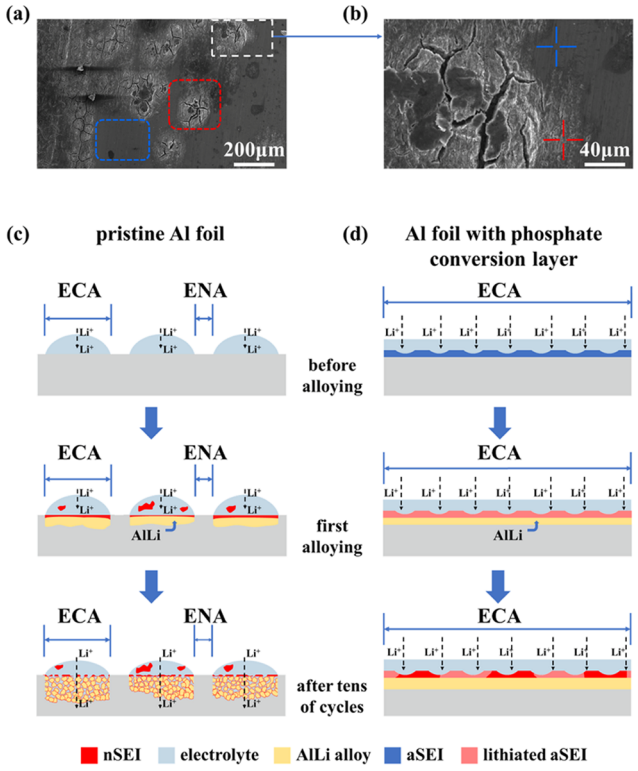

Figure 1. SEM of (a) pristine Al foil anode and (b) enlarged view of pristine Al foil after 7 cycles. Red/blue represents the wetted/unwetted region. (Corresponding EDS analyses for Figure 1b are shown in Figure S1.) Schemes of surface evolution of (c) pristine Al foil and (d) photosphated Al foil anodes.

diffusion distance and readily promote lithiation/delithiation dynamics. However, too big ECA usually leads to more side reactions and higher amount of electrolyte decomposition, which consumes both electrolyte and active lithium, and consequently make the full-cell batteries die quickly because of cyclable lithium- or/and solvent-exhaustion. Therefore, for electrode applications, there should be an optimum granularity, from which the foil anode apparently deviates, and is on the coarser side. Unfortunately, poor electrolyte wettability on foil electrodes makes the situation even worse. As illustrated in Figure 1c, because of the partially wettable foil surface, the electrolyte would only partially cover the anode as pools, instead of spontaneously spreading as an all-covering film. In this case, both the ECA with an access to lithium ions and the electrolyte-free ENA exist. During lithiation, in contrast to ECA regions' enormous dimensional change, the adjacent ENA regions maintain constant volume, which leads to huge internal stress fluctuations and mechanical distortions and cracking of the foil, redistribution of the limited electrolyte, and further exacerbation of ECA/ENA inequality. Note that a passivating solid electrolyte interphase (SEI) layer always forms at the ECA due to the reductive decomposition of liquid electrolytes at the low working potential of Al (<0.5 V vs Li^+/Li) once a fresh conductive surface is exposed to the electrolyte. Such a naturally formed SEI (nSEI) is fragile, breaks off easily, and produces fluffy debris, as the Al foil anode expands and shrinks, which causes continuous electrolyte consumption and an even bigger ECA that also increases electrolyte absorption. In the end, inhomogeneity is further aggravated and damage is localized, leading to gross mechanical and electrical failures.

Herein, we adopt a phosphate conversion coating on an Al foil anode to counteract the above failure mechanism in two aspects: (a) an artificial SEI (aSEI) that is mainly composed of $AlPO_4$ is formed in situ and its strong adherence to the substrate as well as the nSEI largely stabilizes the electrode/electrolyte interface. (b) the $AlPO_4$ layer also improves electrolyte wetting and eliminates the ENA so that uniform lithiation/delithiation is ensured. As illustrated in Figure 1d, after phosphate conversion coating, the electrolyte could readily spread across the Al surface and homogenous

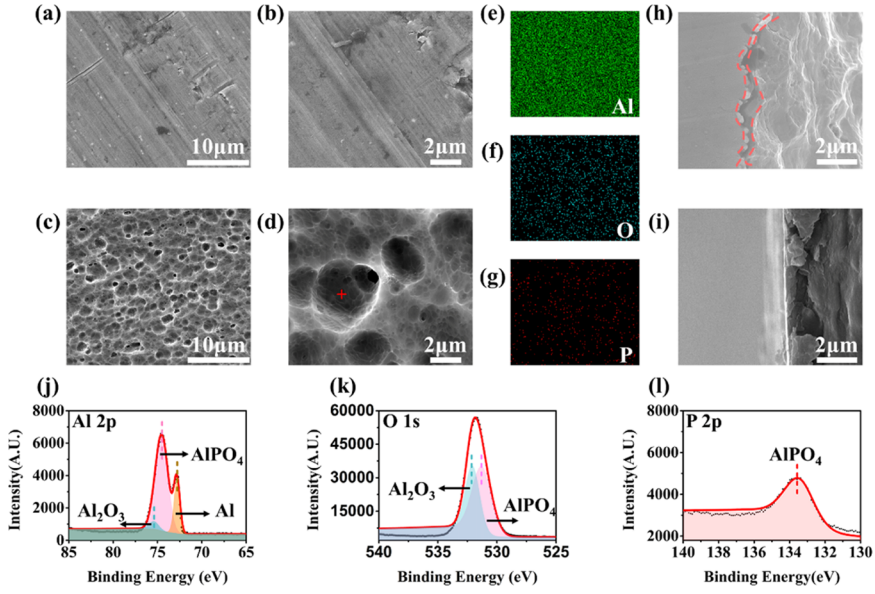

Figure 2. SEM images of the pristine Al foil surface (a) at low magnification and (b) at high magnification, (c) the phosphated Al foil surface at low magnification (d) at high magnification. The phosphated Al mapping image of the (e) Al element, (f) O element, and (g) P element. Cross-sectional SEM of (h) pristine Al foil and (i) phosphated Al foil. (j) XPS for the Al (2p) spectrum of phosphated Al foil. (k) XPS for the O (1s) spectrum of phosphated Al foil. (l) XPS for the P (2p) spectrum of phosphated Al foil.

DOI: 10.1021/acsami.9b02813
ACS Appl. Mater. Interfaces 2019, 11, 15656−15661

expansion/contraction of the Al anode efficiently suppresses gross mechanical failure to guarantee "steady-state" cycling.

By pairing the phosphated Al anode against a commercial $LiFePO_4$ (LFP) cathode with an areal capacity of 2.65 mAh/cm^2, full-cell cycling for 120 times was achieved at a current density of 0.88 mA/cm^2 (The assembling details for the full cell are shown in Table S1). Besides, through careful examination, we found that soluble redox mediators (SRM)[6,7] were released into the electrolyte and shuttled between two electrodes, which explains the discrepancy between the real capacity loss and calculated capacity loss from Coulombic inefficiency (CI) summation.

2. RESULTS AND DISCUSSION

To make a phosphate conversion coating, the Al foil anode was treated by H_3PO_4 aqueous solution, where the following reactions are anticipated to take place[8]

$$Al + H_2PO_4^- \rightarrow AlPO_4 + 2H^+ + 3e \quad (1)$$

$$Al_2O_3 + 2H_2PO_4^- + 2H^+ \rightarrow 2AlPO_4 + H_2O \quad (2)$$

After such a treatment, $AlPO_4$ would be coated on the surface. As indicated in Figure 2, not only the surface component but also the morphology has been changed by the phosphate conversion coating. Compared with the pristine Al foil (Figure 2a,b), which presents a relatively smooth and flat surface, the phosphated Al foil shows a rough surface with uniformly distributed pits (Figure 2c,d). From the EDS mapping, the existence of Al, P, and O (Figure 2e−g) was confirmed. The cross-sectional SEM images (Figure 2h,i) indicate that there were conspicuous regular concave pits and an aSEI layer of ∼1 μm thickness covering the surface. Furthermore, X-ray photoelectron spectroscopy (XPS) is performed to analyze the surface elements and their corresponding valence of phosphated Al foil. Consistent with EDS results, Al, P, and O were detected (Figure 2j−l). The Al 2p peaks at 75.4 and 72.8 eV (Figure 2j) are in correspondence with the reported values of Al_2O_3[9] and the Al substrate.[9] The Al 2p at 74.5 eV is in good agreement with the reported values for $AlPO_4$ film[10,11] and $AlPO_4$ bulk[12,13] samples. Furthermore, in Figure 2k, the O 1s spectra at 532.1 eV is attributed to Al_2O_3,[14] and the peak at 531.9 eV is consistent with the chemical environment of $AlPO_4$.[1313] The P 2p peak at 133.4 eV is consistent with the reported value of amorphous $AlPO_4$[15] (Figure 2l). We anticipate that the metallic aluminum might come from the unreacted surface[16−18] (Figure S2), which indicates that the phosphate conversion coating on Al foil might be not that uniform so far and therefore should be further improved in the future. It is reasonable to conclude that the surface layer mainly consists of $AlPO_4$ and Al_2O_3.

Then, we investigated the wettability of those two Al foil anodes. While the contact angle of the pristine Al foil is 35.2°, it decreases to 15.9° after phosphate treatment (Figure 3a,3b), indicating that electrolyte wetting was enhanced for the phosphated Al anodes. The precise reason for such an enhancement is not clear yet, and it is highly possible that the $AlPO_4$ coating works synergically with the rough surface morphology to improve the apparent wetting angle. When the liquid electrolyte was dropped off on the surface of pristine Al foil, there was a visual localization of the electrolyte (Figure 3c, Video S1), indicating that both the ECA and ENA would appear in cells. In contrast, with an equal amount of the liquid electrolyte on the phosphated Al anode, no ENA could be

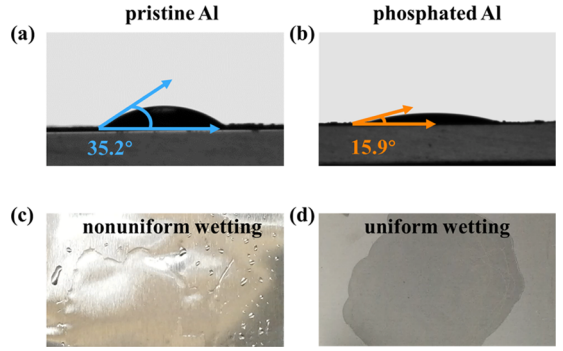

Figure 3. Contact angle between the surface of (a) pristine Al foil and (b) phosphated Al foil and the electrolyte. Electrolyte spreading on the surface of (c) pristine Al foil and (d) phosphated Al foil.

observed (Figure 3d, Video S2). As discussed in Figure 1, the existence of ENA would lead to inhomogeneous alloying reaction and subsequent acceleration of gross failure. On the other hand, the complete spreading-over of the electrolyte on the phosphated Al anode significantly facilitates the homogenous volume expansion/shrinkage during charging−discharging cycles and thus better electrochemical performance should be achieved.

Gassing, which has been confirmed in graphite,[19−21] silicon,[22,23] and tin anodes (unpublished reference),[26] also exists in the Al anode. As shown in Figure S3, gassing can be monitored by in situ differential electrochemical mass spectrometry. For Al//Li half cells, gassing is apparent during the alloying stage. The generated gas bubbles would stick on the surface of Al foil, which cuts off the Li-ion transporting channels. For pristine Al foil, it sticks to the surface tightly. In contrast, the phosphated Al foil with greater liquid wettability helps the generated gas bubbles to detach from the surface quickly (Supporting Information Figure S4, and Videos S3 and S4). The difference in newly formed gas bubble stability would further influence the electrolyte/electrode contact and eventually affect mechanical breaking and spallation of the SEI, as illustrated in Figure 1c.

The electrochemical performance of Al foil anodes was examined in both Al//Li half cells and LFP//Al full cells. From the voltage profile (Figure S5) of the Al//Li half cell, the plateaus at 0.30 and 0.41 V correspond to $Al + Li^+ + e^- \rightarrow LiAl$ (0.30 V vs Li^+/Li) and $LiAl \rightarrow Al + Li^+ + e^-$ (0.41 V vs Li^+/Li), respectively. Meanwhile, in the LFP//Al full cell, during charging, the following reactions occur: $LiFePO_4 \rightarrow Li_{1-x}FePO_4 + xLi^+ + xe^-$ (3.44 V vs Li^+/Li) and $Al + Li^+ + e^- \rightarrow LiAl$ (0.30 V vs Li^+/Li); during discharging, $Li_{1-x}FePO_4 + xLi^+ + xe^- \rightarrow LiFePO_4$ (3.39 V vs Li^+/Li) and $LiAl \rightarrow Al + Li^+ + e^-$ (0.41 V vs Li^+/Li). The CE of such alloying reactions is 99.5% (Figure S6), indicating the reversibility of the alloying reaction of lithium and aluminum at the anode side. As demonstrated in Figure 4a, the average Coulombic efficiency (CE) of the pristine Al anode and phosphated Al anode at 0.5C is 99.02% and 99.15%, respectively. Besides the CE improvement, the phosphated Al anode seems to reduce the polarization voltage compared with the pristine Al anode (Figure S7), indicating an improved electrolyte/electrode contact. The increasing Coulombic efficiency is affected by gassing behavior that originated from electrolyte decomposition (Figure S3). The generated gas bubbles would first absorb on the surface of the Al foil anode, which would inevitably isolate the active material from the electrolyte and then make

DOI: 10.1021/acsami.9b02813
ACS Appl. Mater. Interfaces 2019, 11, 15656−15661

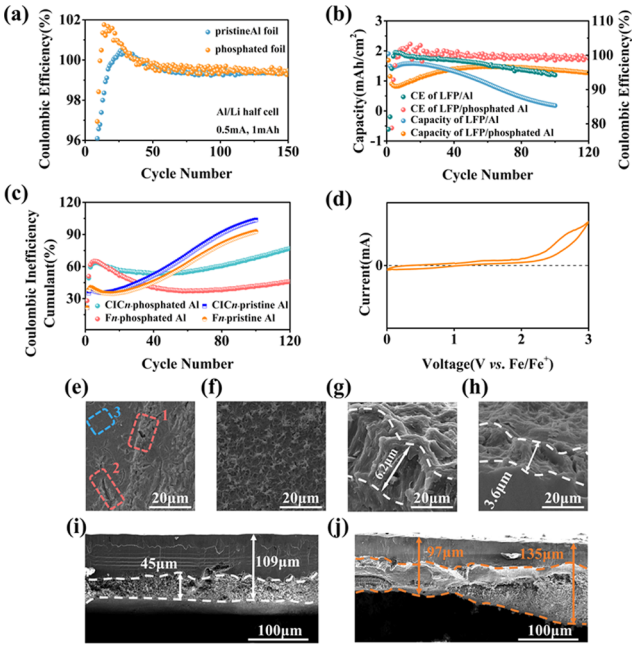

Figure 4. (a) Coulombic efficiency of the Al//Li cell with pristine Al foil or phosphated Al foil. (b) Long cycle performance of the LFP//Al cell with pristine Al foil or phosphated Al foil (areal capacity of the LFP cathode is 2.65 mAh/cm^2). (c) Comparison between CIC$_n$ and F$_n$ of full cells. (d) Cyclic voltammetry (CV) for the steel//steel cell with the recycled electrolyte between 0 and 3 V with a scan rate of 0.1 mV/s. (e) Top-view SEM image of pristine Al foil and (f) top-view SEM image of phosphated Al foil after one cycling in an Al//Li half cell. Corresponding side-view SEM images of (g) pristine Al and (h) phosphated Al foil after one cycling. (i) Side-view SEM image of phosphated Al foil in LFP//Al full cells after ∼120 cycles. (j) Side-view SEM image of pristine Al foil in LFP//Al full cells after ∼120 cycles.

the local lithiated Al inactive temporarily. With prolonged cycling, the absorbed gas bubbles detached and thus the inaccessible area became active again, rendering an increasing Coulombic efficiency. Compared to the pristine Al foil anode, the phosphated Al foil has better wettability to the electrolyte, facilitating gas bubble desorption from the surface and therefore higher CE was observed. Besides, by pairing a commercial LFP cathode (areal capacity of 2.65 mAh/cm^2) against Al foil anodes, we evaluate full-cell cycling before and after phosphate conversion coating. As revealed in Figure 4b, the phosphated Al foil anode exhibits better cycling stability than the pristine Al anode. At a current density of 0.885 mA/cm^2 (from the second cycle, and the initial current density is 0.221 mA/cm^2), the average CE of the full cell with a phosphated Al foil anode is 99.02% in 80 cycles, whereas the LFP//pristine Al presents a lower average CE of 97.74%. Even after 120 cycles, the average CE of the full cells with a phosphated anode is 99.11%. The cell with the phosphated Al foil anode presents a lower polarization voltage (Figure S8), which is consistent with the results obtained for half cells (Figure S7).

However, after close examination of the CE, it is important to note that the real capacity retention fraction after 120 cycles is 54% of its initial capacity (2.65 mAh/cm^2), higher than $(99.11\%)^{120}$ = 34%. We further measure the Coulombic inefficiency cumulant (CIC) that represents the capacity loss calculated based on electron transport monitored by external circuit and capacity fade fraction (F) that is defined as the true discharge capacity loss fraction in LFP//Al full cells without any initial lithium excess.[6] When cycling for 100 cycles, F$_n$ for phosphated Al foil is 42%, much lower than that of pristine Al foil with F$_n$ (93%). The corresponding areal capacity of phosphated Al foil is 1.4 mAh/cm^2, greatly higher than that of pristine Al foil of 0.18 mAh/cm^2. As indicated in Figure 4c, there is an apparent discrepancy between the CIC$_n$ and F$_n$ curves (n represents the nth cycle), especially for the phosphated Al foil. The CIC$_n$ after 120 cycles is ∼77%, much higher than the F$_n$ value of ∼46%. Thus, the actual outcome is more optimistic than what the Coulombic inefficiency cumulant predicts. We hypothesize that there might be SRM during cycling. To verify this hypothesis, cyclic voltammetry (CV) is performed with the used electrolyte in LFP//Al full cells after one cycle. A new separator is used to collect the electrolyte and is resembled into a stainless steel//stainless steel cell. With a fresh electrolyte, there is a "capacitor-like" curve.[7] With the recycled electrolyte, however, an unbalanced charge integral exists as indicated in Figure 4d, which shows that soluble redox species are produced during full-cell cycling. The actual capacity loss (∼46%) after 120 cycles should correspond to a nominal Coulombic efficiency of 99.5%, an excellent value in full cells compared to other metallic foils, such as lithium anodes.[24]

Postmortem microstructures of pristine and phosphated Al foils cycled in full and half cells were examined. For the LFP//Al full cells with a pristine Al foil anode, local areas show large reaction depth with thickness changing from the initial 96 to ∼135 μm after 120 cycles (Figure 4j). However, the thickness changes from the initial 80 to 109 μm uniformly for phosphated Al (Figure 4i). This proves that phosphated Al foil undergoes spatially more uniform electrochemical alloying with lithium. The Al//Li half cells (charging/discharging 0.885 mAh/cm^2) show similar results. From Figure 4e,f, one could observe a significant difference even through only cycled once in half cells. For pristine Al, localization of the electrochemical reaction is obvious: some areas do not react and retain the original surface (area 3 in Figure 4e), whereas other regions show cracked mudlike bumps (area 1 and area 2 in Figure 4e). Conversely, one could observe a continuous and uniform reaction surface for the phosphated Al foil (Figure 4f). Also, a striking contrast is revealed in the corresponding cross-sectional SEM images, and the thickness gain for pristine Al foil is ∼6.2 μm, which is higher than its counterpart phosphated foil, ∼3.6 μm (Figure 4g,h). To learn about the spatial uniformity of thickness growth after longer cycling, a coefficient of variation (C_V) is computed, describing the variance for thickness growth at different locations.[25] As indicated in Figure S9, C_V for pristine Al foil after 10 cycles is 3.0−3.3%, in contrast to 1.5−2% for phosphated Al foil. Lower C_V means more uniform thickness increment. Besides, as shown in Figure S10, impedance of pristine Al is much larger than that of phosphated Al foil. This indicates that the phosphated coating facilitates a stable composite SEI with a lithiated aSEI and nSEI, which enables strong binding with each other as well as with the Al matrix. For pristine Al foil, nSEI can be easily broken and even isolated from the matrix, which leads to further consumption of the electrolyte and active lithium. These results, including low and uniform thickness increment, together with uniform surface and small impedance, demonstrate that phosphated Al possesses less

DOI: 10.1021/acsami.9b02813
ACS Appl. Mater. Interfaces 2019, 11, 15656−15661

ENA and more stable composite SEI (aSEI + nSEI), which turns into better electrochemical performance.[6]

As a matter of fact, the capacity loss is still significant for industrial applications. Therefore, we developed a roll-to-roll prelithiation technology and ~4 mAh/cm^2 (Figure S11) was prelithiated into Al foil, which corresponds to 1.5× Li excess. We then achieved 84% capacity retention after 95 cycles (Figure S12). Within the preliminary attempt for Al foil with the prelithiation process, the high lithium loss in the first cycle was largely compensated and the initial CE was improved from 72% to 91% (Figure S13). Moreover, the stabilized areal capacity is boosted to 2.2 mAh/cm^2 after prelithiation (Figure S12). For Al foil, in the future, the approach might boost Al foil industrialization as anodes in LIBs. Based on the estimation in the Supporting Information, for the same areal capacity of 2.65 mAh/cm^2, 40 μm thick prelithiated Al foil would be sufficient, cutting down 25% volume compared to the graphite anode. Besides, compared to other alternative self-supporting anodes, such as graphene paper, the Al foil anode has much better electrical conductivity and mechanical properties. Also, the free-standing Al foil anode eliminates the usage of the Cu foil current collector, the cost of which (~\$10 kg^{-1}) is much higher than Al (~\$2 kg^{-1}). Additionally, some inactive components like binders and conductive agents could also be waived, so that the industrial production is largely simplified as well.

3. CONCLUSIONS

In conclusion, we proved the existence of an ENA in a bare Al foil anode, which obviously degrades the electrochemical performance. To eliminate such a destructive phenomenon, a phosphate conversion coating was adopted, which turns out to improve the electrolyte wettability and promote gas bubble detachment, and thus the electrolyte fully spreads over the Al anode to ensure a uniform alloying reaction. After such a treatment, the phosphated Al foil achieves full-cell cycling with 1.27 mAh/cm^2 after 120 cycles. The in situ generated $AlPO_4$ layer also works as an aSEI to facilitate stronger binding between the compound SEI and matrix, promoting the stability of the SEI. Therefore, a uniform reaction area was ensured. A large part of the full-cell capacity loss comes from the low initial Coulombic efficiency, so we will try prelithiation to enhance the properties further. The phosphate conversion coating on a self-supporting metallic foil anode is a cheap and general industrial process, which can be easily scaled up and provides a practical strategy to improve the electrochemical performance of metallic foil anodes in LIBs.

■ ASSOCIATED CONTENT

Supporting Information

The Supporting Information is available free of charge on the ACS Publications website at DOI: 10.1021/acsami.9b02813.

Experimental section, materials characterization, electrochemical measurements, gassing measurements, parameters of individual components in LFP//Al full cells (PDF)

Electrolyte spreading (AVI) (AVI)

Gas bubble desorption (AVI) (AVI)

■ AUTHOR INFORMATION

Corresponding Authors

*E-mail: lisa@tongji.edu.cn (S.L.).

*E-mail: liju@mit.edu (J.L.).

ORCID

Ju Li: 0000-0002-7841-8058

Author Contributions

The manuscript was written through contributions of all authors. All authors have given approval to the final version of the manuscript.

Notes

The authors declare no competing financial interest.

■ ACKNOWLEDGMENTS

This work was financially supported by the National Natural Science Foundation of China (NSFC—No. 51602222 and No. 51632001).

■ REFERENCES

(1) Hamon, Y.; Brousse, T.; Jousse, F.; Topart, P.; Buvat, P.; Schleich, D. M. Aluminum Negative Electrode in Lithium Ion Batteries. *J. Power Sources* **2001**, *97*−*98*, 185−187.

(2) Li, S.; Niu, J.; Zhao, Y. C.; So, K. P.; Wang, C.; Wang, C. A.; Li, J. High-rate Aluminium Yolk-shell Nanoparticle Anode for Li-ion Battery with Long cycle Life and Ultrahigh Capacity. *Nat. Commun.* **2015**, *6*, No. 7872.

(3) Liu, Y.; Hudak, N. S.; Huber, D. L.; Limmer, S. J.; Sullivan, J. P.; Huang, J. Y. In Situ Transmission Electron Microscopy Observation of Pulverization of Aluminum Nanowires and Evolution of the Thin Surface Al_2O_3 Layers during Lithiation−Delithiation Cycles. *Nano Lett.* **2011**, *11*, 4188−4194.

(4) Ji, B.; Zhang, F.; Sheng, M.; Tong, X.; Tang, Y.; Novel, A. A Novel and Generalized Lithium-Ion-Battery Configuration utilizing Al Foil as Both Anode and Current Collector for Enhanced Energy Density. *Adv. Mater.* **2016**, *29*, No. 1604219.

(5) Li, S.; Li, Q.; Carpick, R. W.; Gumbsch, P.; Liu, X. Z.; Ding, X.; Sun, J.; Li, J. The Evolving Quality of Frictional Contact with Graphene. *Nature* **2016**, *539*, 541.

(6) Jin, Y.; Li, S.; Kushima, A.; Zheng, X.; Sun, Y.; Xie, J.; Sun, J.; Xue, W.; Zhou, G.; Wu, J.; Shi, F.; Zhang, R.; Zhu, Z.; So, K.; Cui, Y.; Li, J. Self-healing SEI Enables Full-cell Cycling of a Silicon-majority Anode with a Coulombic Efficiency Exceeding 99.9%. *Energy Environ. Sci.* **2017**, *10*, 580−592.

(7) Zheng, Y.; Lu, Y.; Qi, X.; Wang, Y.; Mu, L.; Li, Y.; Ma, Q.; Li, J.; Hu, Y.-S. Superior Electrochemical Performance of Sodium-ion Full-cell Using Poplar Wood Derived Hard Carbon Anode. *Energy Storage Mater.* **2018**, 269−279.

(8) Kuo, H.-S.; Tsai, W.-T. Effects of Alumina and Hydrogen Peroxide on the Chemical-mechanical Polishing of Aluminum in Phosphoric Acid Base Slurry. *Mater. Chem. Phys.* **2001**, *69*, 53−61.

(9) Riggs, W. M.; Parker, M. J. Chapter 4 - Surface Analysis by X-ray Photoelectron Spectroscopy. In *Methods of Surface Analysis*; Czanderna, A. W., Ed.; Elsevier: Amsterdam, 1975; pp 103−158.

(10) Appapillai, A. T.; Mansour, A. N.; Cho, J.; Shao-Horn, Y. Microstructure of $LiCoO_2$ with and without "$AlPO_4$" Nanoparticle Coating: Combined STEM and XPS Studies. *Chem. Mater.* **2007**, *19*, 5748−5757.

(11) Kim, B.; Kim, C.; Ahn, D.; Moon, T.; Ahn, J.; Park, Y.; Park, B. Nanostructural Effect of $AlPO_4$-nanoparticle Coating on the Cycle-life Performance in $LiCoO_2$ Thin Films. *Electrochem. Solid State Lett.* **2007**, *10*, A32−A35.

(12) Wu, F.; Zhang, X.; Zhao, T.; Li, L.; Xie, M.; Chen, R. Multifunctional $AlPO_4$ Coating for Improving Electrochemical Properties of Low-cost $Li[Li_{0.2}Fe_{0.1}Ni_{0.15}Mn_{0.55}]O_2$ Cathode Materials for Lithium-ion Batteries. *ACS Appl. Mater. Interfaces* **2015**, *7*, 3773−3781.

(13) Rotole, J. A.; Sherwood, P. M. A. Aluminum Phosphate by XPS. *Surf. Sci. Spectra* **1998**, *5*, 60−66.

DOI: 10.1021/acsami.9b02813
ACS Appl. Mater. Interfaces 2019, 11, 15656−15661

(14) Chen, C.; Splinter, S. J.; Do, T.; McIntyre, N. S. Measurement of Oxide Film Growth on Mg and Al Surfaces over Extended Periods Using XPS. *Surf. Sci.* **1997**, *382*, L652−L657.
(15) Campelo, J. M.; Jaraba, M.; Luna, D.; Luque, R.; Marinas, J. M.; Romero, A. A.; Navio, J. A.; Macias, M. Effect of Phosphate Precursor and Organic Additives on the Structural and Catalytic Properties of Amorphous Mesoporous $AlPO_4$ Materials. *Chem. Mater.* **2003**, *15*, 3352−3364.
(16) Burstein, G. T.; Cinderey, R. J. The Potential of Freshly Generated Metal Surfaces Determined from the Guillotined Electrode—A New Technique. *Corros. Sci.* **1991**, *32*, 1195−1211.
(17) Prabhu, D.; Rao, P. *Coriandrum sativum* L. A Novel Green Inhibitor for the Corrosion Inhibition of Aluminium in 1.0M Phosphoric Acid Solution. *J. Environ. Chem. Eng.* **2013**, *1*, 676−683.
(18) Kuo, H. S.; Tsai, W. T. Electrochemical Behavior of Aluminum during Chemical Mechanical Polishing in Phosphoric Acid Base Slurry. *J. Electrochem. Soc.* **2000**, *147*, 149−154.
(19) Michalak, B.; Berkes, B. B.; Sommer, H.; Bergfeldt, T.; Brezesinski, T.; Janek, J. Gas Evolution in $LiNi_{0.5}Mn_{1.5}O_4$/Graphite Cells Studied In Operando by a Combination of Differential Electrochemical Mass Spectrometry, Neutron Imaging, and Pressure Measurements. *Anal. Chem.* **2016**, *88*, 2877−2883.
(20) Metzger, M.; Strehle, B.; Solchenbach, S.; Gasteiger, H. A. Origin of H_2 Evolution in LIBs: H_2O Reduction vs. Electrolyte Oxidation. *J. Electrochem. Soc.* **2016**, *163*, A798−A809.
(21) Starke, B.; Seidlmayer, S.; Schulz, M.; Dinter, A.; Revay, Z.; Gilles, R.; Pettinger, K.-H. Gas Evolution and Capacity Fading in $LiFe_xMn_{1-x}PO_4$/Graphite Cells Studied by Neutron Imaging and Neutron Induced Prompt Gamma Activation Analysis. *J. Electrochem. Soc.* **2017**, *164*, A3943−A3948.
(22) Schiele, A.; Breitung, B.; Hatsukade, T.; Berkes, B. B.; Hartmann, P.; Janek, J.; Brezesinski, T. The Critical Role of Fluoroethylene Carbonate in the Gassing of Silicon Anodes for Lithium-Ion Batteries. *ACS Energy Lett.* **2017**, *2*, 2228−2233.
(23) Ruther, R. E.; Hays, K. A.; An, S. J.; Li, J.; Wood, D. L.; Nanda, J. Chemical Evolution in Silicon−Graphite Composite Anodes Investigated by Vibrational Spectroscopy. *ACS Appl. Mater. Interfaces* **2018**, *10*, 18641−18649.
(24) Suo, L.; Xue, W.; Gobet, M.; Greenbaum, S. G.; Wang, C.; Chen, Y.; Yang, W.; Li, Y.; Li, J. Fluorine-donating Electrolytes Enable Highly Reversible 5-V-class Li Metal Batteries. *Proc. Natl. Acad. Sci. U.S.A.* **2018**, *115*, 1156−1161.
(25) Abdi, H. *Coefficient of variation*, SAGE Publications: Thousand Oaks, California, 2010; Vol. *1*, pp 169−171.
(26) Xu, H.; Li, S.; Zhang, C.; Chen, X.; Liu, W.; Zheng, Y.; Xie, Y.; Huang, Y.; Li, J. Roll-to-roll Prelithiation of Sn Foil Anode Suppresses Gassing and Enables Stable Full-cell Cycling of Lithium Ion Batteries. 2019.

DOI: 10.1021/acsami.9b02813
ACS Appl. Mater. Interfaces 2019, 11, 15656−15661